Mechanically Interlocked Linkers inside Metal–Organic Frameworks: Effect of Ring Size on Rotational Dynamics

ARTICLE *in* JOURNAL OF THE AMERICAN CHEMICAL SOCIETY · AUGUST 2015

Impact Factor: 12.11 · DOI: 10.1021/jacs.5b04674

7 AUTHORS, INCLUDING:

Vedran Nicholas Vukotic
PROTO Manufacturing
24 PUBLICATIONS **431** CITATIONS
SEE PROFILE

Kelong Zhu
University of Windsor
32 PUBLICATIONS **883** CITATIONS
SEE PROFILE

Robert Schurko
University of Windsor
108 PUBLICATIONS **1,993** CITATIONS
SEE PROFILE

JACS
JOURNAL OF THE AMERICAN CHEMICAL SOCIETY
Article
pubs.acs.org/JACS

Mechanically Interlocked Linkers inside Metal–Organic Frameworks: Effect of Ring Size on Rotational Dynamics

V. Nicholas Vukotic, Christopher A. O'Keefe, Kelong Zhu, Kristopher J. Harris, Christine To, Robert W. Schurko,* and Stephen J. Loeb*

Department of Chemistry and Biochemistry, University of Windsor, Windsor, Ontario, Canada N9B 3P4

Supporting Information

ABSTRACT: A series of metal–organic framework (MOF) materials has been prepared, each containing a mechanically interlocked molecule (MIM) as the linker and a copper(II) paddlewheel as the secondary building unit (SBU). The MIM linkers are [2]rotaxanes with varying sizes of crown ether macrocycles ([22]crown-6, **22C6**; [24]crown-6, **24C6**; [26]-crown-6, **26C6**; benzo[24]crown-6, **B24C6**) and an anilinium-based axle containing four carboxylate donor groups. Herein, the X-ray structures of MOFs **UWCM**-1 (no crown) and **UWDM-1**$_{(22)}$ are compared and demonstrate the effect of including a macrocycle around the axle of the linker. The rotaxane linkers are linear and result in nbo-type MOFs with void space that allows for motion of the interlocked macrocycle inside the MOF pores, while the macrocycle-free linker is bent and yields a MOF with a novel 12-connected bcc structure. Variable temperature ^{2}H solid-state nuclear magnetic resonance showed that the macrocycles in **UWDM-1**$_{(22)}$, **UWDM-1**$_{(24)}$, and **UWDM-1**$_{(B24)}$ undergo different degrees and rates of rotation depending on the size and shape of the macrocycle.

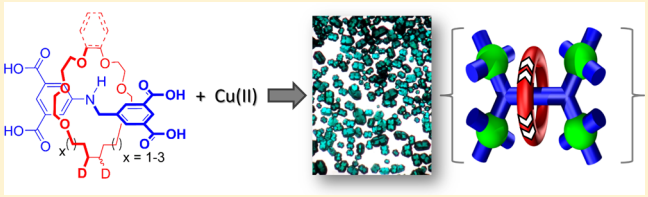

1. INTRODUCTION

The synthesis of mechanically interlocked molecules (MIMs)[1] and the study of the relative motion of their constituent components have resulted in a variety of molecular rotors,[2] shuttles,[3] switches,[4] and sophisticated molecular machines.[5] The vast majority of these studies, however, are performed in solution where the molecules are in a constant state of flux and are randomly dispersed. The ability to organize these molecules in high density, while still allowing the free volume required for them to operate, is a key step in producing materials in which the physical properties of the material can be tuned at the molecular level and potentially creating ultradense molecular-based memory.

The incorporation of MIMs into crystalline three-periodic coordination polymers or metal–organic frameworks (MOFs)[6] allows for a high level of molecular organization. To date, pseudorotaxane linkers, as well as a few interlocked catenane and rotaxane linkers, have been utilized to incorporate MIMs into one-, two-, and three-periodic frameworks.[7] We recently reported a prototype material, University of Windsor Dynamic Material (**UWDM-1**),[8] which demonstrated the first example of a macrocyclic component of a MIM being able to rapidly rotate inside of a MOF material. Removing solvent from the pores of the MOF created the free volume required for the macrocyclic component of the MIM to undergo rapid thermally driven rotation of the macrocycles, as observed directly by variable temperature (VT) ^{2}H solid-state nuclear magnetic resonance (SSNMR) spectroscopy.

Herein, we report the synthesis and characterization of (1) a series of MIMs utilizing a benzyl-aniline based axle with various macrocyclic wheels, (2) a body-centered cubic (bcc)-type MOF constructed from the macrocycle-free linker (MIM axle) and Cu^{II} metal ions demonstrating the effect the macrocycle has on the shape of the linker, and ultimately the type of MOF obtained, and (3) an isomorphous series of MIM in MOF materials (**UWDM-1**) with various sized macrocycles and the corresponding dynamics of the macrocyclic component as characterized by VT ^{2}H SSNMR.

2. RESULTS AND DISCUSSION

MIM Linker Synthesis and Characterization. Scheme 1 outlines the synthetic protocol for all of the MIM linkers utilized in this study. Compound **1** has two very specific design features which were chosen for their compatibility with both MIM and MOF synthesis. First, it contains a benzyl-aniline-based axle which can be protonated to form a benzyl-anilinium cation and is a known recognition site for crown ether-based macrocycles.[9] This core is also relatively short and compact in order to minimize framework flexibility and ultimately improve the stability of the resulting MOF. Second, the terminal diethyl 3,5-benzene-dicarboxylate groups are designed to act as large stoppers to prevent the macrocyclic ring from slipping off the axle while simultaneously improving the solubility of the axle during MIM synthesis; subsequent hydrolysis of the ethyl esters results in terminal isophthalic acid groups which are well-known coordinating ligands in MOF synthesis.[10]

Received: May 5, 2015
Published: July 15, 2015

DOI: 10.1021/jacs.5b04674
J. Am. Chem. Soc. 2015, 137, 9643–9651

Scheme 1. Synthesis of MIMs Utilizing Various Macrocyclic Precursors and a Macrocycle-Free Linker[a]

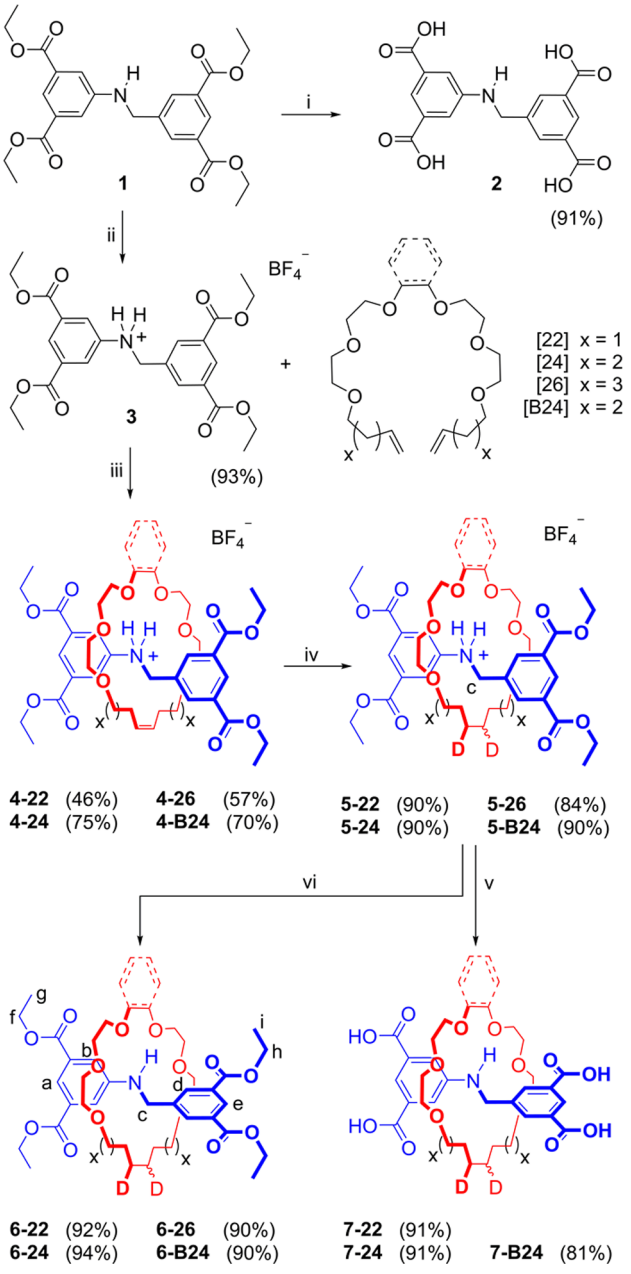

[a](i) 2 M NaOH, MeOH/THF, 24 h, 80 °C; (ii) HBF_4, Et_2O; (iii) Grubbs' first-generation catalyst, $MeNO_2/CH_2Cl_2$, 48 h, 42 °C; (iv) 10% Pd/C, D_2, MeOH (or MeOH/THF), RT, 1−24 h; (v) 2 M NaOH, MeOH/THF, 24 h, 80 °C; (vi) $NaHCO_3$, CH_2Cl_2/H_2O.

Protonation of **1** with HBF_4 produces benzyl-anilinium axle **3**, which we have shown to be a good recognition site for a ring-closing metathesis (RCM) reaction using Grubbs' first-generation catalyst and a 24-membered crown ether macrocyclic precursor.[8] In order to explore the versatility of this template and ultimately to determine what effect changing the macrocycle size would have on the dynamics of the MIM when incorporated into a MOF, different sized macrocyclic precursors were used in the RCM reaction (Scheme 1). The template proved efficient for synthesis of rotaxanes (as *E* and *Z* isomers) with a smaller 22-membered macrocycle (**4-22**) in 46% yield, a larger 26-membered macrocycle (**4-26**) in 57% yield, and a 24-membered macrocycle with a benzene moiety (**4-B24**) in 70% yield. The variation in the yield of the RCM reaction can be thought of as a reflection of the overall strength of the interaction between **3** and the macrocyclic precursor coupled with the ability of the catalyst to efficiently perform the RCM reaction. This correlates reasonably well with the fact that **4-24** has the best yield (75%) when compared to **4- 22**, which has increased ring strain, **4-26**, which has longer more flexible terminal alkyl olefins, and **4-B24**, with the benzene moiety which pulls electron density away from the crown ether oxygen atoms making them slightly weaker hydrogen-bond acceptors.

Reduction of the remaining olefin group on rotaxanes **4-22**, **4-24** , **4-26**, and **4-B24** allowed for inclusion of a deuterium (^2H) tag which was used to study the dynamics of the macrocycle in the solid state, *vide infra*. This was accomplished by reduction with deuterium gas over palladium on carbon to produce rotaxanes **5-22**, **5-24**, **5-26**, and **5-B24** in good yield (84−90%). Figure 1 shows the ^1H NMR spectrum of **5-24** and

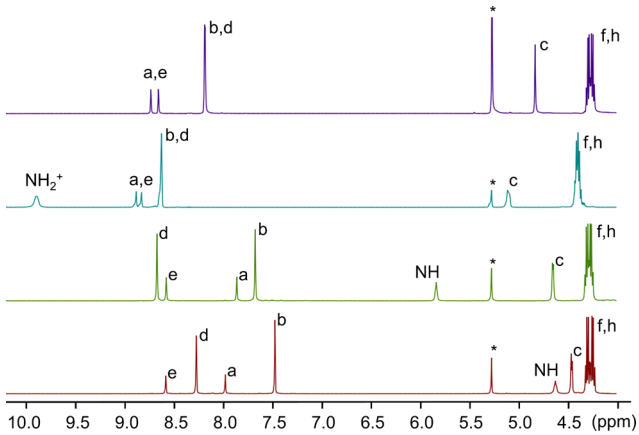

Figure 1. ^1H NMR spectra (500 MHz, 300 K, CD_2Cl_2) from top to bottom: protonated axle **3** (NH_2^+ resonance not observed), protonated rotaxane **5-24**, neutral rotaxane **6-24**, and neutral axle **1**. See Scheme 1 for labeling of protons.

the downfield shifts of axle protons due to hydrogen bonding with the macrocyclic wheel in comparison to the protonated axle **3**. Facile deprotonation of these rotaxanes was possible by dissolving the rotaxanes in CH_2Cl_2 followed by stirring with an aqueous sodium bicarbonate solution to produce neutral rotaxanes **6-22**, **6-24**, **6-26**, and **6-B24** in good yield (90−94%). The decreased basicity of the aniline group compared to secondary amine-based rotaxanes, which are known to be difficult to deprotonate,[11] was another critical design feature which allowed for elimination of a majority of the noncovalent templating interactions originally used to form the [2]rotaxane. This dramatically reduces the interaction between axle and wheel, thus maximizing the freedom of the macrocyclic component of the MIM to undergo motion. The ^1H NMR spectra in Figure 1 depict the significant change in the chemical shifts−e.g. NH_2^+ of **5-24** (δ = 9.82 ppm) and neutral NH of **6-24** (δ = 5.85 ppm) corresponding to the reduced acidity of the NH proton(s).

Although deprotonation greatly reduces the interaction between axle and wheel, there remains a measurable hydrogen-bonding interaction as signified by the downfield shifts of the NH and benzyl CH_2 resonances in the ^1H NMR spectra of neutral rotaxanes **6-22**, **6-B24**, **6-24**, **6-26**, when compared to the neutral axle **1** (Figure 2). Analysis of the spectroscopic and

DOI: 10.1021/jacs.5b04674
J. Am. Chem. Soc. 2015, 137, 9643−9651

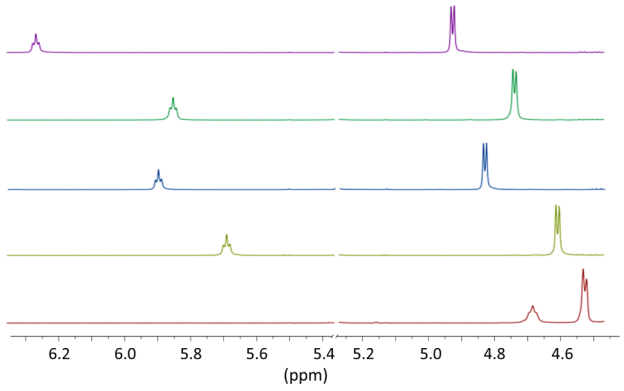

Figure 2. ^{1}H NMR spectra (500 MHz, 300 K, CD_2Cl_2) top to bottom showing NH (triplet) and CH_2 (doublet) resonances for neutral rotaxanes **6-22**, **6-24**, **6-B24**, **6-26**, and neutral axle **1**. Residual $CDHCl_2$ solvent peak omitted for clarity.

structural data of these ethyl ester MIMs allows for a better understanding of the noncovalent interactions that must be broken in order for the macrocyclic component to rotate about the axle when incorporated into MOFs.

The shifts of the NH and benzyl CH_2 resonances can be correlated to the size of the macrocycle; a smaller macrocycle shows a greater downfield shift, inferring an increase in hydrogen-bonding strength between the MIM components. The ^{1}H NMR spectrum of **6-22** exhibits the greatest downfield shift of the NH (δ = 6.27 ppm) and CH_2 resonances (δ = 4.93 ppm), which correlates with the short NH···O (3.18 Å, ∠(NHO) = 156°) and CH···O (3.19 Å, ∠(CHO) = 145° and 134°) contacts in the crystal structure (Figure 3). The smaller ring size of **6-22** also results in the aromatic groups of the axle being almost coplanar with a dihedral angle of 7.6° which maximizes the interactions between the axle and the macrocycle.

Increasing the macrocycle size by two atoms in **6-24** results in an upfield shift of the NH (δ = 5.90 ppm) and CH_2 resonances (δ = 4.83 ppm), corresponding to reduced hydrogen bonding in comparison to **6-22**. The crystal structure of **6-24** shows a NH···O interaction of 3.09 Å, (∠(NHO) = 177°) and a single long CH···O distance of 3.49 Å, (∠(CHO) = 147°). In comparison, while **6-B24** also has a 24-membered macrocycle, the addition of the pendent benzene moiety reduces the flexibility of the macrocycle and results in slightly downfield shifts of the NH (δ = 5.85 ppm) and CH_2 resonances (δ = 4.74 ppm), which correlates with shorter NH···O (3.05 Å, ∠(NHO) = 136°) and CH···O (3.42 Å, ∠(CHO) = 138°) distances in the crystal structure (Figure 3). In addition, the larger 24-membered macrocycles have much larger dihedral angles between the aromatic substituents on the axle, becoming almost perpendicular in **6-24** and **6-B24**, with dihedral angles of 63° and 84°, respectively (Figure 3). In comparison, **6-26**, which has the largest 26-membered macrocyclic ring, shows the most upfield chemical shifts of the NH (δ = 5.69 ppm) and CH_2 (δ = 4.61 ppm) resonances, corresponding to the weakest hydrogen-bonding interactions between the macrocycle and the axle (Figure 2).

Hydrolysis of the ethyl ester groups of **5-22**, **5-24**, and **5-B24** results in tetracarboxylic acid MIM linkers **7-22**, **7-24**, and **7-B24** (Scheme 1). Unfortunately, when **5-26** was subjected to hydrolysis, the loss of the ethyl ester groups resulted in unthreading of the 26-membered macrocyclic ring from the

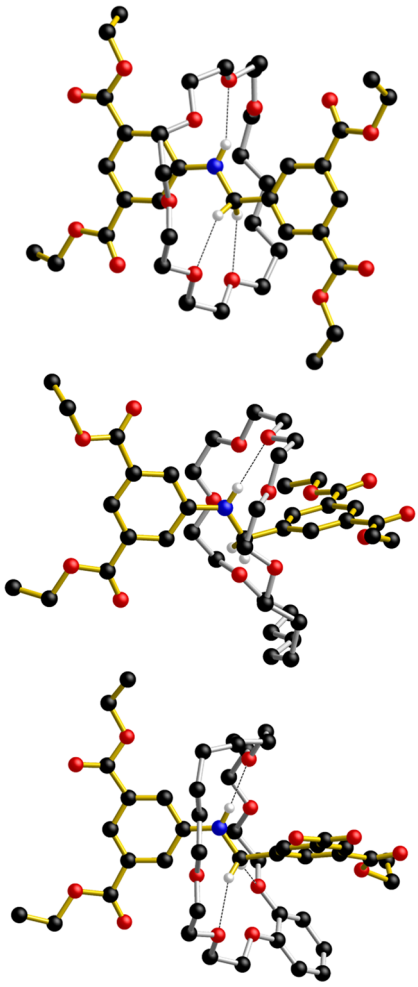

Figure 3. Ball-and-stick representations of the single-crystal X-ray structures, top to bottom: neutral rotaxanes **6-22**, **6-24**, and **6-B24**. Color key: C = black, O = red, N = blue, H = white.

axle, indicating that isophthalic acid is not a large enough stopper for this size of macrocycle.

MOF Synthesis and Characterization. In order to determine what effect, if any, the macrocyclic ring has on the MOF topology obtained, naked linker **2** was prepared by hydrolysis of **1** (Scheme 1). Linker **2** was then combined with $Cu(NO_3)_2{\cdot}H_2O$ in a 3:2:2 mixture of DMF/EtOH/H_2O with two drops of HNO_3 and heated to 65 °C for 48 h in a temperature-controlled oven (Scheme 2). This resulted in a green crystalline material that was designated as **UWCM-1**.

Analysis of **UWCM-1** by single-crystal X-ray diffraction (XRD) showed the material to have an overall formula of $[Cu_6(\mathbf{2})_3(DMF)_4(H_2O)_2]{\cdot}(DMF)x$, and crystallize in tetragonal space group $I4/m$, (yield 77%). The terminal 1,3-benzenedicarboxylate groups of linker **2** coordinate to the Cu^{II} metal ions to form dimeric Cu^{II} paddlewheel units (Figure 4 top) which assemble into cuboctahedral cages (nanoballs)[12] consisting of 12 paddlewheel units comprising 24 Cu^{II} ions and 24 iso-phthalate groups, with an internal diameter of 16.0 Å between metal centers. The nanoballs can be described as possessing small rhombihexahedron topology and O_h symmetry[13] arising from the 12 square paddlewheel units which generate eight triangular windows and six square windows (Figure 4 bottom).[14]

DOI: 10.1021/jacs.5b04674
J. Am. Chem. Soc. 2015, 137, 9643−9651

Scheme 2. Solvothermal Synthesis with MIM Linkers 7-22, 7-24, and 7-B24 and Naked Linker 2[a]

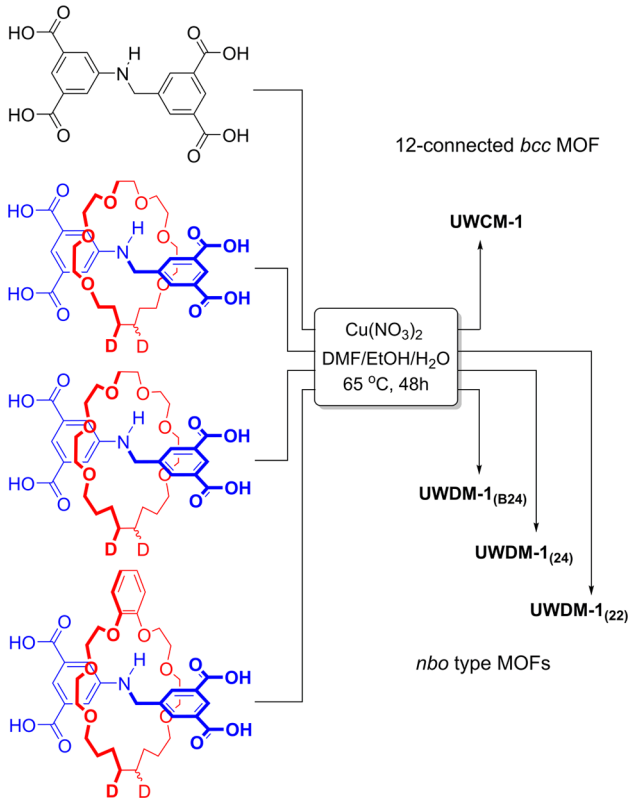

[a]When linkers **2**, **7-22**, **7-24** , and **7-B24** are used under identical synthetic conditions, naked linker **2** produces a bcc-type MOF topology (**UWCM-1**), while MIM linkers **7-22**, **7-24**, and **7-B24** form isomorphous nbo-type MOFs **UWDM-1**$_{(22)}$, **UWDM-1**$_{(24)}$ and **UWDM-1**$_{(B24)}$.

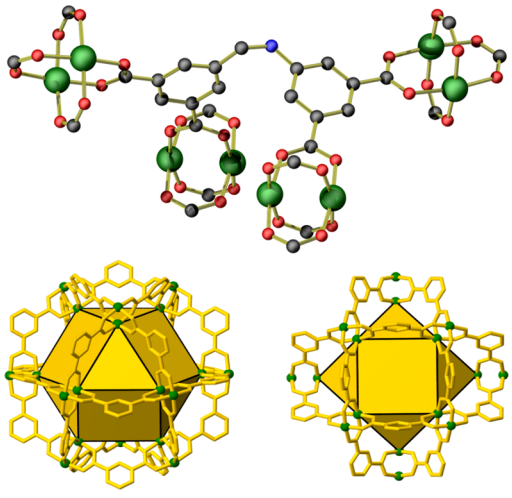

Figure 4. Top: ball-and-stick representation of the major geometric isomer of naked linker **2** within **UWCM-1**, coordinated to four paddlewheel units, hydrogen atoms and coordinated solvent molecules omitted for clarity. Color key: C = black, O = red, N = blue, Cu = green. Bottom left: view down one of the eight triangular windows of a nanoball, consisting of 12 Cu^{II} paddlewheel units and 24 iso-phthalate groups. Bottom right: view down one of the six square windows of a nanoball. Skeleton of the nanoball shown with gold bonds, while linking of the internal Cu^{II} ions results in a cuboctahedron represented by gold panels.

It has previously been shown that flexible linkages at the 5-position between 1,3-benzenedicarboxylate moieties result in cross-linked nanoball MOFs in which connections are made via the six square windows, resulting in a primitive cubic pcu net.[12b,13,15] In these MOFs, four linkages are made at each of the six square windows to satisfy the 24 possible connections. It was previously noted in the literature that of the 24 possible connections, double connections between nanoballs were unlikely because of the orientation of the decoration sites;[12b] however, **UWCM-1** accomplishes just this.

Each Cu_{24} nanoball is connected to its 12 nearest neighbors via two links, resulting in a non-interpenetrated 12-connected net. This is made possible by the fact that there are two crystallographically independent linkers of **2** which occur in a 2:1 ratio. The major geometric isomer is severely bent and makes two links to each of the four nanoballs, above and below the plane, for a total of 16 links (Figure 5). The minor geometric isomer is less bent and makes two links to each of the four nanoballs in the plane, resulting in the remaining eight

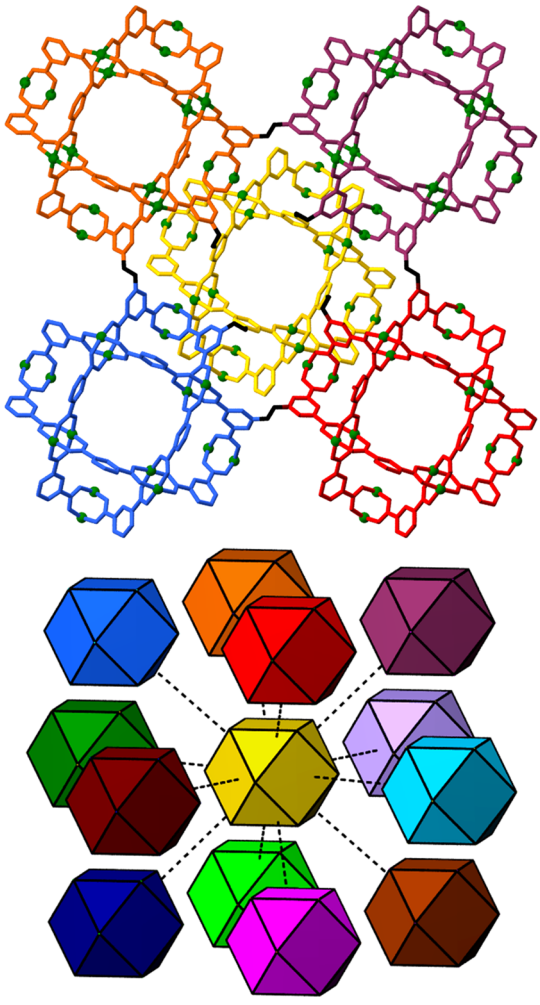

Figure 5. Top: view down the *c*-axis of **UWCM-1**, depicting how the central nanoball (yellow) is linked to four nanoballs above the plane (red, blue, orange, and purple) via the major isomer of **2**, while the minor isomer of **2** links nanoballs which fall in the same plane. Cu metal ions are shown in green, and links between nanoballs are shown in black. Bottom: a schematic showing how the nanoballs (depicted as cuboctahedra) are linked to form a body-centered cubic 12-connected net.

DOI: 10.1021/jacs.5b04674
J. Am. Chem. Soc. 2015, 137, 9643−9651

links to satisfy all 24 possible linkages. The overall packing of the Cu_{24} nanoballs can be described as bcc, in which each nanoball is connected to four other nanoballs above and four below (25.2 Å between nanoball centers), in addition to four slightly elongated contacts in plane (26.1 Å between nanoball centers), resulting in connections to 12 other nanoballs to form a unique 12-connected net. While the arrangement of nanoballs within the structure is bcc, the underlying topology of this framework could be described as fcu if each nanoball with 24 potential points of extension is considered as a 12-connected node and the two linkages between each nanoball thought of as a single connection point.[12c,d]

Within the structure of **UWCM-1**, the square window openings of the nanoballs align to form channels along the *c*-axis with a diameter of 11.2 Å (Figure 5). DMF and water solvent molecules occupy the axial coordination sites on the Cu_2 paddlewheel units, resulting in the interior sites of each nanoball containing eight coordinated DMF molecules and four coordinated water molecules, while the exterior sites also coordinate to eight DMF molecules and four water molecules. Removal of axial and interstitial solvent molecules results in a solvent accessible volume of 68% as calculated by PLATON.[16]

In contrast to **UWCM-1**, the reaction of a MIM linker (**7-22**, **7-24**, or **7-B24**) with $Cu(NO_3)_2{\cdot}H_2O$ under exactly the same synthetic conditions leads to the formation of an isomorphous series of MIM in MOF materials (**UWDM-1**) with various sized macrocycles.[8] Single-crystal XRD of **UWDM-1**$_{(22)}$ determined the formula to be $[Cu_2(\mathbf{7\text{-}22})(H_2O)_2]{\cdot}4(H_2O)$ in trigonal space group *R*3. The terminal 1,3-benzenedicarboxylate groups of **7-22** coordinate to Cu^{II} metal ions to form dimeric Cu_2 paddlewheel units (Figure 6) which assemble into distorted octahedral cages consisting of six paddlewheel units, comprising 12 Cu^{II} ions, with an internal diameter of 12.4 Å between metal centers (Figure 6). The overall topology of the framework is a rare β-phase of nbo topology.[17] In comparison to MOFs, which form the α-phase of nbo , a unique feature of the β-phase is that it results in larger pores along the *c*-axis, maximizing the distance between the bulky macrocyclic rings of MIM linker **7-22** . This may be a driving force for the formation of the β-phase, as no α-phase has been observed to form with any of the MIM linkers. The macrocyclic component of the MIM linker also works to rigidify the flexible $-NHCH_2-$ link between iso-phthalate groups. While flexible linkages at the 5-postions of iso-phthalate groups are known to result in linked nanoball structures similar to **UWCM-1**, rigid aromatic linkers are known to result in nbo-type MOFs[10] similar to **UWDM-1**$_{(22)}$.

The small amount of void space within the structure (17%) is occupied by interstitial water molecules in addition to those bound to the axial sites on the paddlewheel units. The stability of **UWDM-1**$_{(22)}$ was determined by thermogravimetric analysis (TGA) and powder X-ray diffraction (PXRD), which showed the material to be stable up to ~200 °C.

It was unknown whether the smaller size of the 22-membered ring of MIM linker **7-22** or the bulker size of the benzo-24-membered ring of MIM linker **7-B24** would affect the type of MOF topology obtained. However, under the same synthetic conditions, altering the ring size resulted in formation of **UWDM-1**$_{(22)}$ (77% yield) and **UWDM-1**$_{(B24)}$ (67% yield), both of which exhibited the same MOF structure as **UWDM-1**$_{(24)}$ (75% yield) as shown by PXRD (Figure 7).

Interestingly, while large single crystals of **UWDM-1**$_{(22)}$ and **UWDM-1**$_{(24)}$ were easily grown and analyzed by single crystal XRD, only microcrystalline powder samples of **UWDM-1**$_{(B24)}$ were obtained, under identical synthetic conditions. Analysis by scanning electron microscopy (SEM) revealed that **UWDM-1**$_{(B24)}$ formed small microcrystalline rosettes (see Figure S-47). It may be that the bulky size of the benzo-24-membered macrocycle results in defects during the crystallization process, preventing the formation of larger crystals. However, this could also be attributed to a simple difference in solubility between linkers, due to the additional aromatic substituent on the macrocycle in MIM linker **7-B24**. Analysis of **UWDM-1**$_{(B24)}$ by

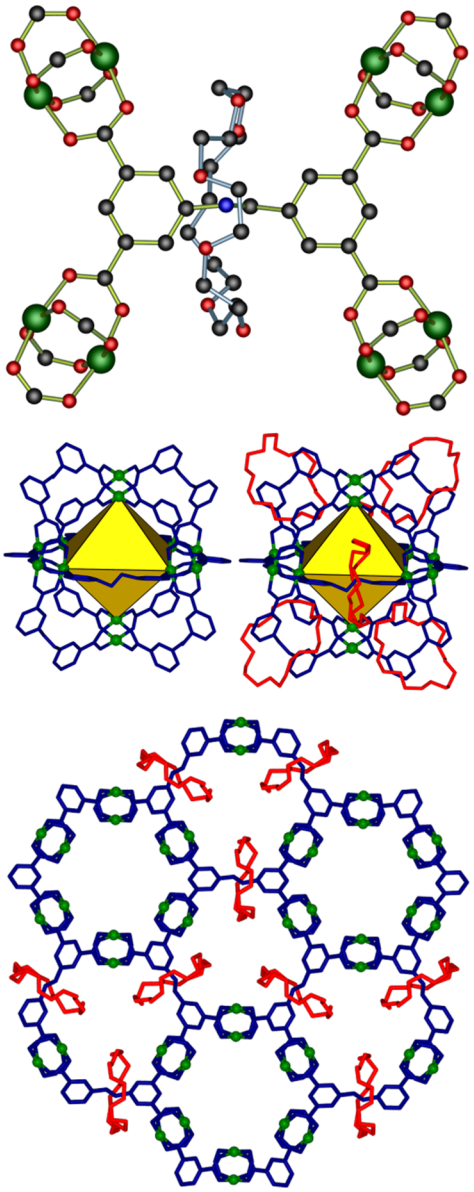

Figure 6. Top: ball-and-stick representation of MIM linker **7-22** coordinated to four paddlewheel units in **UWDM-1**$_{(22)}$ (hydrogen atoms and solvent molecules omitted for clarity; color key, C = black, O = red, N = blue, Cu = green. Middle left: stick representation of the distorted octahedral cage consisting of six Cu^{II} paddlewheel units with macrocycles omitted; Middle right: same but with macrocycles shown. Bottom: view down the *c*-axis of **UWDM-1**$_{(22)}$ depicting the hexagonal shaped channels (framework shown in blue, macrocycles in red and Cu^{II} metal ions in green; hydrogen atoms and solvent molecules omitted for clarity).

DOI: 10.1021/jacs.5b04674
J. Am. Chem. Soc. 2015, 137, 9643−9651

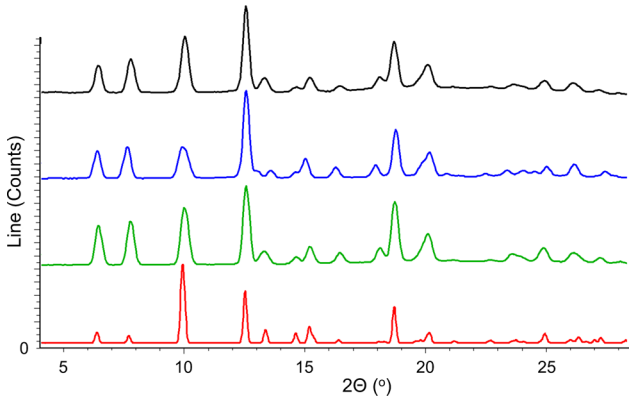

Figure 7. PXRD patterns, top to bottom: **UWDM-1**$_{(22)}$, **UWDM-1**$_{(24)}$, **UWDM-1**$_{(B24)}$, simulated from the crystal structure of **UWDM-1**$_{(24)}$.

TGA and PXRD showed the material to have similar stability to **UWDM-1**$_{(22)}$ and **UWDM-1**$_{(24)}$.

Dynamics of UWDM-1 Series in the Solid State. The macrocycles in the **UWDM-1** series were prepared with deuterium labels through the addition of D_2 to the double bond (Scheme 1). The resulting MOF materials were then probed by ^{2}H SSNMR to determine the types of motion each macrocyclic ring was undergoing. In this section, a detailed description of the motional models that were previously proposed for **UWDM-1**$_{(24)}$ is given,[8] then the dynamics of the new **UWDM-1**$_{(22)}$ and **UWDM-1**$_{(B24)}$ are discussed, compared, and contrasted with those of **UWDM-1**$_{(24)}$. A brief overview of the general theory of ^{2}H SSNMR, as well as more detailed discussion of the modes of motion, can be found in the Supporting Information (SI).

^{2}H SSNMR is aptly suited to the study of dynamics on the molecular level and can provide detailed information on the modes of motion and their respective rates.[18] Three motional regimes are defined based on the relative magnitudes of the ^{2}H quadrupolar frequency (ν_Q) and the exchange rate (ν_{ex}): the slow motion limit (SML), where rates are $<10^3$ Hz ($\nu_{ex} \ll \nu_Q$), the intermediate motion regime (IMR), where rates are between 10^4 and 10^7 Hz ($\nu_{ex} \approx \nu_Q$), and the fast motion limit (FML) where rates are $>10^7$ Hz ($\nu_{ex} \gg \nu_Q$). The powder patterns corresponding to rates in the SML and FML can be modeled using motionally averaged ^{2}H electric-field gradient (EFG) tensors and are invariant to changes in both echo spacing and temperature. Motions with rates in the IMR produce complex powder patterns that change with echo spacing and temperature. The VT ^{2}H SSNMR spectra, simulations, and depictions of the modes of motion in **UWDM-1**$_{(24)}$, **UWDM-1**$_{(22)}$, and **UWDM-1**$_{(B24)}$ are depicted in Figure 8.

The low-temperature spectrum of **UWDM-1**$_{(24)}$ acquired at 160 K was simulated as a single site with quadrupolar parameters: C_Q = 160(5) kHz and η_Q = 0.0(1); these parameters are typical for a deuteron bonded to a carbon atom in an alkyl group. The spectrum was simulated with rates in the SML, and therefore, the motion does not influence the appearance of the powder pattern. Increasing the temperature to 225 K produces no appreciable changes in the powder patterns. The spectrum acquired at 251 K is drastically different from the lower temperature spectra, and this was simulated

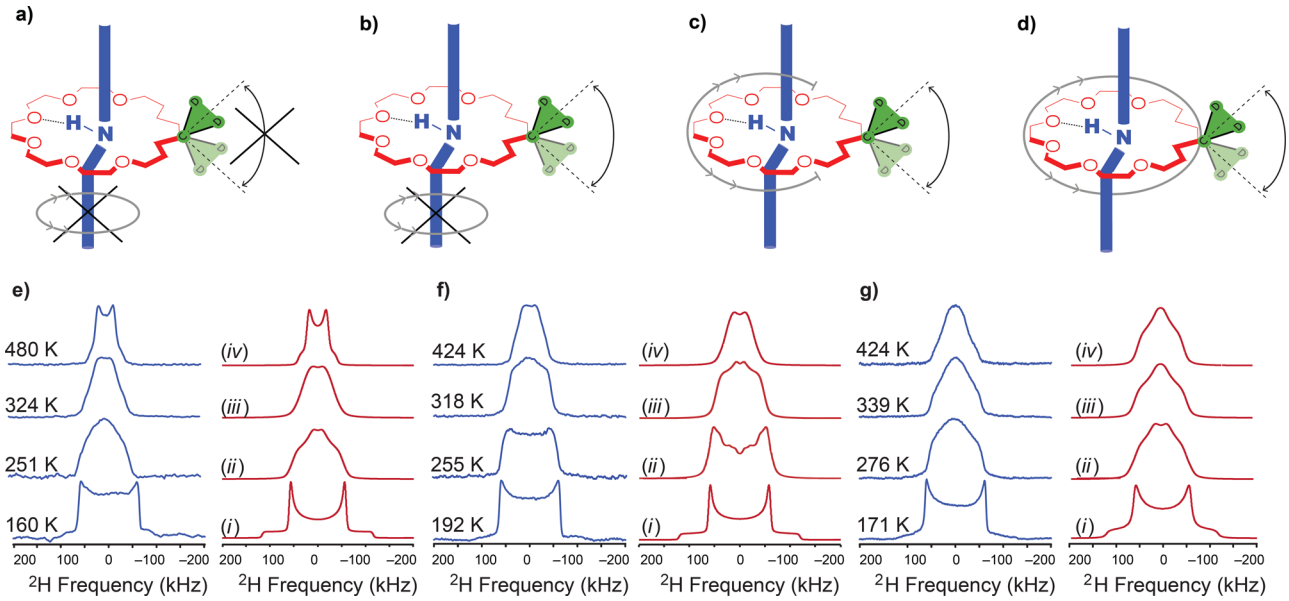

Figure 8. Schematic representation of the possible modes of motion of the macrocyclic rings within the **UWDM-1** series: (a) no motion of the macrocyclic ring, (b) two-site jump of the CD_2 groups, (c) partial rotation of the macrocycle about the six ether oxygen atoms within the ring, in addition to the two-site jump of the CD_2 groups, (d) full rotation of the macrocyclic ring, in addition to the two-site jump of the CD_2 groups. Experimental ^{2}H VT SSNMR powder patterns (blue) and corresponding analytical simulations (red) for (e) **UWDM-1**$_{(24)}$ where (i) motions are occurring at rates within the SML and do not affect the appearance of the powder pattern, (ii) two-site jumps through an angle of 77°, (iii) two-site jumps through 60° combined with partial rotation of the ring in 45° steps through 225°, and (iv) two-site jumps through 70° combined with full, rapid rotation of the ring; (f) **UWDM-1**$_{(22)}$ where (i) motions are at rates within the SML and do not affect the appearance of the powder pattern, (ii) two-site jumps of the deuterons through an angle of 65° with rates in the IMR, (iii) two-site jumps with the onset of partial rotation of the ring in 50° steps through 250°, and (iv) two-site jumps and partial rotation occurring at rates within the FML; and (g) **UWDM-1**$_{(B24)}$ where (i) motions are at rates within the SML and do not affect the appearance of the powder pattern, (ii) two-site jumps through an angle of 60°, (iii) two-site jumps through an angle of 65°, and (iv) two-site jumps through an angle of 75°.

DOI: 10.1021/jacs.5b04674
J. Am. Chem. Soc. 2015, 137, 9643−9651

based upon a two-site jump of the deuteron through an angle of 77°. The two-site jump mode of motion consists of the deuterons of the CD_2 groups jumping between two positions that are related by a rotation through an angle β about an axis that is perpendicular to the plane of the CD_2 moiety and produces powder patterns that are dependent on β (Figure S-53).[19] The spectrum acquired at 324 K could not be simulated using solely the two-site jump model and, instead, was simulated using the partial rotation model, combined with two-site jumps with β = 60°. The partial rotation model consists of the macrocyclic ring rotating about an axis that is perpendicular to the ring in steps separated by the angle γ. The jumps are made only to adjacent sites that allow for the interaction of the hydrogen-bond donor on the axle with the oxygen atoms on the ring (Figure S-55). The high-temperature spectrum collected at 480 K is axially symmetric (i.e., $\eta_Q = 0$) and cannot be simulated with the partial rotation model but instead was simulated as full rotation,[20] combined with two-site jumps with β = 60°. The macrocyclic ring is no longer constrained to making jumps between adjacent oxygen atoms on the ring but now has enough energy to jump through the alkyl portion in either direction. The full-rotation was simulated with rates within the FML, and while it is difficult to comment on the relative rates of the full rotation and two-site jump motional models, it is postulated that the latter is occurring at a higher rate, due to its significantly lower onset temperature.

To determine whether a smaller macrocyclic ring size would result in a more constrained (i.e., less mobile) ring, or if the larger free volume resulting from the smaller ring size would in fact result in a less constrained (i.e., more mobile) ring, VT ^{2}H SSNMR experiments and analytical simulations of **UWDM-1**$_{(22)}$ were undertaken (Figure 8f). The spectrum acquired at 192 K was simulated as a single site and as the static case where any motions that are occurring are at rates within the SML. Increasing the temperature produces subtle changes in the powder patterns; this was simulated by considering the two-site jump mode of motion with β = 65° and rates within the IMR. The rates of the two-site jump continue to increase as the temperature is raised, with the onset of the FML at 318 K. The spectra acquired at temperatures of 276 K and above were simulated with the onset of partial rotation combined with the two-site jumps. The smaller macrocyclic ring size in this system means that the six rotation sites, corresponding to the different hydrogen-bonding oxygen atoms, are separated by a larger angle with respect to the rotation axis (i.e., γ = 50° for **UWDM-1**$_{(22)}$ and 45° for **UWDM-1**$_{(24)}$. The spectra acquired at 276 and 297 K were simulated with rates in the IMR for both the two-site jumps and partial rotation modes. The FML for the two-site jump is reached at 318 K, whereas the rates for the partial rotation continue to increase until the FML is reached at 424 K. It is noted that there is no evidence for full rotation when the high-temperature limit is reached, as the spectrum is not axially symmetric.

UWDM-1$_{(B24)}$ incorporates a bulky **B24C6** macrocycle, which might be expected to have significantly hindered motion in comparison to the previous two systems. Ratcliffe et al. examined a similar system in their study of the dynamics in carboxybenzo[24]crown-8 and its KNCS complexes.[19] They found that rotation was not possible, and the only motion present was two-site jumps with jump angle increasing with temperature. A similar model was used in the simulation of the dynamics of **UWDM-1**$_{(B24)}$ (Figure 8g, Figure S-57). The spectra acquired at 171 and 198 K were simulated with rates within the SML, whereas the spectrum acquired at 213 K shows subtle changes in comparison to the lower temperature spectra and was simulated with the onset of the two-site jump motion. The spectra up to 276 K were simulated with rates within the IMR and a jump angle of 60°. The FML for the two-site jump was reached at 297 K with a jump angle of 60°. Increasing the temperature further results in an increase in the jump angle, and the high-temperature spectrum acquired at 424 K was simulated with a jump angle of 75° and rates in the FML. There was no evidence of rotation, either partial or full, for this system.

The macrocycles in **UWDM-1**$_{(24)}$ are certainly the most mobile of the series studied, indicating that the **24C6** macrocycle provides both ample free volume and limited interaction with the axle. The FML for the two-site jump motion is reached at approximately 251 K, partial rotation at 324 K, and full rotation at 423 K and above. In comparison, for the smaller 22-membered ring inside **UWDM-1**$_{(22)}$ the FML for the two-site jump motion is not reached until 318 K, which is almost 70 K higher than for **UWDM-1**$_{(24)}$. The higher onset temperature and smaller jump angle suggest the smaller **22C6** macrocyclic ring in **UWDM-1**$_{(22)}$ is undergoing a much more hindered motion than that of the **24C6** macrocycle. This claim is further substantiated when the partial rotation model is considered. The onset of partial rotation occurs at 276 K, similar to **UWDM-1**$_{(24)}$, and the FML is reached by about 400 K. The spectrum acquired in the high-temperature limit (424 K) was also simulated using the partial rotation model, and there is no evidence of full rotation. This is in contrast to **UWDM-1**$_{(24)}$, where evidence of full rotation is manifested in the spectrum acquired at 423 K. The hindered two-site jump motion, in addition to no evidence of full rotation, clearly indicates that the larger free volume afforded by a smaller ring size is counteracted by the tighter fit of the macrocyclic ring around the axle.

The macrocycle in the **UWDM-1**$_{(B24)}$ species fits around the axle in a similar manner to that in **UWDM-1**$_{(24)}$; however, the bulky phenyl substituent greatly reduces the free volume and increases interactions between the macrocyclic ring and the framework. It was postulated that the motion in this species would be greatly encumbered and be akin to that observed by Ratcliffe et al. in their study of carboxybenzo[24]crown-8.[19] The only motion observed for this species was the two-site jump with the FML being reached at about 297 K. The higher temperature for the onset of the FML, in comparison to that of **UWDM-1**$_{(24)}$, suggests that the bulkier macrocyclic ring significantly hinders the conformational changes in the ring associated with the two-site jump. Furthermore, the absence of rotation (either partial or full) verifies the restricted nature of the macrocyclic ring in this species.

The three distinct motional modes in the **UWDM-1** series occur in sequential stages. While it may be desirable to calculate activation energies for each of the individual modes of motion, this is difficult due to the presence of multiple, simultaneous modes of motion occurring at different rates. The first mode of motion that occurs in all systems is the two-site jump, with the FML being reached at 251, 318, and 297 K for **UWDM-1**$_{(24)}$, **UWDM-1**$_{(22)}$, and **UWDM-1**$_{(B24)}$, respectively. The onset temperature of the two-site jump motion is dependent on both the fit of the macrocycle around the axle and the overall steric bulk of the macrocyclic ring. Second, provided there is sufficient free volume, partial rotation occurs, and the jump angle depends on the size of the ring. This mode of motion

DOI: 10.1021/jacs.5b04674
J. Am. Chem. Soc. 2015, 137, 9643−9651

occurs for both **UWDM-1**$_{(24)}$ and **UWDM-1**$_{(22)}$ with FML temperatures of 324 and 424 K, respectively. Finally, only for the **24C6** macrocycle in **UWDM-1**$_{(24)}$ is full rotation of the ring possible, with the FML being reached at 423 K.

3. CONCLUSION

A series of MIM linkers was synthesized containing a common anilinium-based axle and different macrocyclic rings: **22C6**, **24C6**, **26C6**, and **B24C6**. These linkers were used to create an isomorphous series of MIM in MOF materials: **UWDM-1**$_{(22)}$, **UWDM-1**$_{(24)}$, and **UWDM-1**$_{(B24)}$. The **UWDM-1** series form a rare β-phase of nbo-type topology and provide a unique platform to study the motion of different sized and shaped macrocyclic rings within the same solid-state environment.

The most mobile of the series is **UWDM-1**$_{(24)}$ which undergoes three distinct motions: a two-site jump of CD_2 groups, a partial rotation of the macrocyclic ring and full rapid rotation of the ring, reaching the FMLs for these motions at 251, 324, and 423 K respectively. For **UWDM-1**$_{(22)}$, the FML of the two-site jump and partial rotation occurs at temperatures 67 and 100 K higher than the 24-membered ring, and there is no evidence of full rotation. This is consistent with the increased hydrogen-bonding interactions between the 22-membered macrocyclic ring and the axle, as seen in the solution ^{1}H NMR spectra and the crystal structure of **6-22**, resulting in a less mobile system in the solid state. In contrast, **UWDM-1**$_{(B24)}$ reached the FML for the two-site jump at 297 K and showed no evidence of full or partial rotation. The bulky benzo group of the macrocycle therefore acts as a molecular break, preventing rotation of the macrocycle inside the material.

When an identical linker with no macrocycle was combined with Cu^{II} metal ions under synthetic conditions that were identical to those used to form the **UWDM-1** series, a bcc-type MOF (**UWCM-1**) was formed instead. The structure consisted of Cu^{II} nanoballs linked in a previously unidentified (and purportedly impossible) 12-connected net. This clearly demonstrates the effect the macrocyclic component has on the flexibility of the linker; the ring acts to rigidify the flexible $-NHCH_2-$ link between iso-phthalate groups, thus rigidifying the linker by incorporating it into a MIM. This ultimately changes the type of MOF architecture that can be generated.

We have successfully created an isomorphous series of MIM in MOF materials in which each material exhibits different degrees of motion of the macrocyclic ring. While these systems are under thermal control, which can be used to start and stop rotation of the macrocycles within the framework (Figure 9),

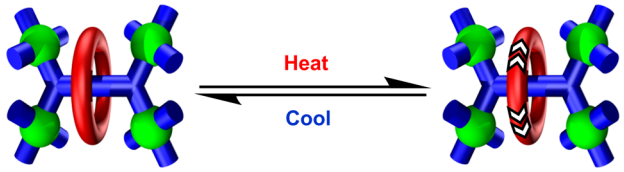

Figure 9. Cartoon illustrating the thermally driven and reversible ring rotation within MOF **UWDM-1**$_{(24)}$.

the future of this research will focus on developing systems that can be controlled photo- or electrochemically and to create systems with cooperative motion in an effort to create functional molecular machines within MOFs.

■ ASSOCIATED CONTENT

Supporting Information

Experimental details describing the synthesis and characterization of all new compounds including solution NMR assignments, full characterization details for all new materials and the details of all SSNMR experiments and simulations. The Supporting Information is available free of charge on the ACS Publications website at DOI: 10.1021/jacs.5b04674.

■ AUTHOR INFORMATION

Corresponding Authors

*loeb@uwindsor.ca
*schurko@uwindsor.ca

Notes

The authors declare no competing financial interest.

■ ACKNOWLEDGMENTS

This work was supported by the Natural Sciences and Engineering Research Council (NSERC) of Canada through Discovery Grants and Accelerator Supplements to S.J.L. and R.W.S. and a Canada Research Chair award to S.J.L. R.W.S. thanks the University of Windsor for a 50th Anniversary Jubilee Chair. R.W.S. and S.J.L. are also grateful for support from NSERC, the Canadian Foundation for Innovation, the Ontario Innovation Trust and the University of Windsor for the development and maintenance of the SSNMR and XRD centers. V.N.V. is grateful for financial support provided by the Natural Sciences and Engineering Research Council of Canada through an Alexander Graham Bell Canada Graduate Doctoral Scholarship and by the International Center for Diffraction Data for a Ludo Frevel Crystallography Scholarship. The authors acknowledge M. Revington for technical assistance with solution NMR spectroscopy experiments and J. Auld for recording electrospray mass spectrometry data. Alexander Stirk of the Loeb research group is acknowledged for collecting the SEM images of the **UWDM-1** series.

■ REFERENCES

(1) (a) Stoddart, J. F. *Chem. Soc. Rev.* **2009**, *38*, 1802. (b) Bruns, C. J.; Stoddart, J. F. *Top. Curr. Chem.* **2012**, *323*, 19. (c) Browne, C.; Ronson, T. K.; Nitschke, J. R. *Angew. Chem., Int. Ed.* **2014**, *53*, 10701. (d) Gil-Ramirez, G.; Leigh, D. A.; Stephens, A. J. *Angew. Chem., Int. Ed.* **2015**, *54*, 6110.

(2) (a) Schalley, C. A.; Beizai, K.; Vogtle, F. *Acc. Chem. Res.* **2001**, *34*, 465. (b) Van Quaethem, A.; Lussis, P.; Leigh, D. A.; Duwez, A. S.; Fustin, C. A. *Chem. Sci.* **2014**, *5*, 1449. (c) Ballesteros, B.; Faust, T. B.; Lee, C. F.; Leigh, D. A.; Muryn, C. A.; Pritchard, R. G.; Schultz, D.; Teat, S. J.; Timco, G. A.; Winpenny, R. E. P. *J. Am. Chem. Soc.* **2010**, *132*, 15435. (d) Nishimura, D.; Oshikiri, T.; Takashima, Y.; Hashidzume, A.; Yamaguchi, H.; Harada, A. *J. Org. Chem.* **2008**, *73*, 2496. (e) Gatti, F. G.; Lent, S.; Wong, J. K. Y.; Bottari, G.; Altieri, A.; Morales, M. A. F.; Teat, S. J.; Frochot, C.; Leigh, D. A.; Brouwer, A. M.; Zerbetto, F. *Proc. Natl. Acad. Sci. U. S. A.* **2003**, *100*, 10. (f) Bermudez, V.; Gase, T.; Kajzar, F.; Capron, N.; Zerbetto, F.; Gatti, F. G.; Leigh, D. A.; Zhang, S. *Opt. Mater.* **2003**, *21*, 39.

(3) (a) Zhu, K. L.; Vukotic, V. N.; Noujeim, N.; Loeb, S. J. *Chem. Sci.* **2012**, *3*, 3265. (b) Zhu, K. L.; Vukotic, V. N.; Loeb, S. J. *Angew. Chem., Int. Ed.* **2012**, *51*, 2168. (c) Zhang, T.; Mu, L.; She, G.; Shi, W. *Chem. Commun.* **2012**, *48*, 452. (d) Panman, M. R.; Bodis, P.; Shaw, D. J.; Bakker, B. H.; Newton, A. C.; Kay, E. R.; Leigh, D. A.; Buma, W. J.; Brouwer, A. M.; Woutersen, S. *Phys. Chem. Chem. Phys.* **2012**, *14*, 1865. (e) Tokunaga, Y.; Kawabata, M.; Matsubara, N. *Org. Biomol. Chem.* **2011**, *9*, 4948. (f) Hanni, K. D.; Leigh, D. A. *Chem. Soc. Rev.* **2010**, *39*, 1240. (g) Lee, C.-F.; Leigh, D. A.; Pritchard, R. G.; Schultz,

DOI: 10.1021/jacs.5b04674
J. Am. Chem. Soc. 2015, 137, 9643−9651

D.; Teat, S. J.; Timco, G. A.; Winpenny, R. E. P. *Nature* **2009**, *458*, 314. (h) Crowley, J. D.; Goldup, S. M.; Lee, A.-L.; Leigh, D. A.; McBurney, R. T. *Chem. Soc. Rev.* **2009**, *38*, 1530.

(4) (a) Bruns, C. J.; Li, J. N.; Frasconi, M.; Schneebeli, S. T.; Iehl, J.; de Rouville, H. P. J.; Stupp, S. I.; Voth, G. A.; Stoddart, J. F. *Angew. Chem., Int. Ed.* **2014**, *53*, 1953. (b) Yang, W.; Li, Y.; Liu, H.; Chi, L.; Li, Y. *Small* **2012**, *8*, 504. (c) Zhang, W. Y.; DeIonno, E.; Dichtel, W. R.; Fang, L.; Trabolsi, A.; Olsen, J. C.; Benitez, D.; Heath, J. R.; Stoddart, J. F. *J. Mater. Chem.* **2011**, *21*, 1487. (d) Suhan, N. D.; Allen, L.; Gharib, M. T.; Viljoen, E.; Vella, S. J.; Loeb, S. J. *Chem. Commun.* **2011**, *47*, 5991. (e) Olsen, J. C.; Fahrenbach, A. C.; Trabolsi, A.; Friedman, D. C.; Dey, S. K.; Gothard, C. M.; Shveyd, A. K.; Gasa, T. B.; Spruell, J. M.; Olson, M. A.; Wang, C.; de Rouville, H. P. J.; Botros, Y. Y.; Stoddart, J. F. *Org. Biomol. Chem.* **2011**, *9*, 7126. (f) Li, H.; Fahrenbach, A. C.; Coskun, A.; Zhu, Z. X.; Barin, G.; Zhao, Y. L.; Botros, Y. Y.; Sauvage, J. P.; Stoddart, J. F. *Angew. Chem., Int. Ed.* **2011**, *50*, 6782. (g) Davidson, G. J. E.; Sharma, S.; Loeb, S. J. *Angew. Chem., Int. Ed.* **2010**, *49*, 4938. (h) Leigh, D. A.; Thomson, A. R. *Tetrahedron* **2008**, *64*, 8411. (i) Loeb, S. J.; Tiburcio, J.; Vella, S. J. *Chem. Commun.* **2006**, 1598.

(5) (a) Coskun, A.; Banaszak, M.; Astumian, R. D.; Stoddart, J. F.; Grzybowski, B. A. *Chem. Soc. Rev.* **2012**, *41*, 19. (b) Baggerman, J.; Haraszkiewicz, N.; Wiering, P. G.; Fioravanti, G.; Marcaccio, M.; Paolucci, F.; Kay, E. R.; Leigh, D. A.; Brouwer, A. M. *Chem. - Eur. J.* **2013**, *19*, 5566. (c) Zhang, Q.; Tu, Y. Q.; Tian, H.; Zhao, Y. L.; Stoddart, J. F.; Agren, H. *J. Phys. Chem. B* **2010**, *114*, 6561. (d) Bodis, P.; Panman, M. R.; Bakker, B. H.; Mateo-Alonso, A.; Prato, M.; Buma, W. J.; Brouwer, A. M.; Kay, E. R.; Leigh, D. A.; Woutersen, S. *Acc. Chem. Res.* **2009**, *42*, 1462. (e) Balzani, V.; Credi, A.; Venturi, M. *Chem. Soc. Rev.* **2009**, *38*, 1542. (f) Huang, T. J.; Flood, A. H.; Brough, B.; Liu, Y.; Bonvallet, P. A.; Kang, S. S.; Chu, C. W.; Guo, T. F.; Lu, W. X.; Yang, Y.; Stoddart, J. F.; Ho, C. M. *IEEE Trans. Autom. Sci. Eng.* **2006**, *3*, 254. (g) Clemente-Leon, M.; Credi, A.; Martinez-Diaz, M. V.; Mingotaud, C.; Stoddart, J. F. *Adv. Mater.* **2006**, *18*, 1291. (h) Berna, J.; Leigh, D. A.; Lubomska, M.; Mendoza, S. M.; Perez, E. M.; Rudolf, P.; Teobaldi, G.; Zerbetto, F. *Nat. Mater.* **2005**, *4*, 704. (i) Perez, E. M.; Dryden, D. T. F.; Leigh, D. A.; Teobaldi, G.; Zerbetto, F. *J. Am. Chem. Soc.* **2004**, *126*, 12210. (j) Balzani, V.; Gomez-Lopez, M.; Stoddart, J. F. *Acc. Chem. Res.* **1998**, *31*, 405. (k) Fasano, V.; Baroncini, M.; Moffa, M.; Iandolo, D.; Camposeo, A.; Credi, A.; Pisignano, D. *J. Am. Chem. Soc.* **2014**, *136*, 14245. (l) Ragazzon, G.; Baroncini, M.; Silvi, S.; Venturi, M.; Credi, A. *Nat. Nanotechnol.* **2014**, *10*, 70. (m) Tayi, A. S.; Kaeser, A.; Matsumoto, M.; Aida, T.; Stupp, S. I. *Nat. Chem.* **2015**, *7*, 281.

(6) (a) Nugent, P.; Belmabkhout, Y.; Burd, S. D.; Cairns, A. J.; Luebke, R.; Forrest, K.; Pham, T.; Ma, S. Q.; Space, B.; Wojtas, L.; Eddaoudi, M.; Zaworotko, M. J. *Nature* **2013**, *495*, 80. (b) Perry, J. J.; Perman, J. A.; Zaworotko, M. J. *Chem. Soc. Rev.* **2009**, *38*, 1400. (c) Li, J. R.; Sculley, J.; Zhou, H. C. *Chem. Rev.* **2012**, *112*, 869. (d) Makal, T. A.; Li, J. R.; Lu, W. G.; Zhou, H. C. *Chem. Soc. Rev.* **2012**, *41*, 7761. (e) Li, J. R.; Zhou, H. C. *Nat. Chem.* **2010**, *2*, 893. (f) Eddaoudi, M.; Kim, J.; Rosi, N.; Vodak, D.; Wachter, J.; O'Keeffe, M.; Yaghi, O. M. *Science* **2002**, *295*, 469. (g) Furukawa, H.; Cordova, K. E.; O'Keeffe, M.; Yaghi, O. M. *Science* **2013**, *341*, 974. (h) Zhang, H. C.; Zou, R. Q.; Zhao, Y. L. *Coord. Chem. Rev.* **2015**, *292*, 74. (i) Gao, W. Y.; Cai, R.; Pham, T.; Forrest, K. A.; Hogan, A.; Nugent, P.; Williams, K.; Wojtas, L.; Luebke, R.; Weselinsk, L. J.; Zaworotko, M. J.; Space, B.; Chen, Y. S.; Eddaoudi, M.; Shi, X. D.; Ma, S. Q. *Chem. Mater.* **2015**, *27*, 2144. (j) Sue, A. C. H.; Mannige, R. V.; Deng, H. X.; Cao, D.; Wang, C.; Gandara, F.; Stoddart, J. F.; Whitelam, S.; Yaghi, O. M. *Proc. Natl. Acad. Sci. U. S. A.* **2015**, *112*, 5591. (k) Lin, Z. J.; Lu, J.; Hong, M. C.; Cao, R. *Chem. Soc. Rev.* **2014**, *43*, 5867. (l) Chen, T. H.; Popov, I.; Kaveevivitchai, W.; Miljanic, O. S. *Chem. Mater.* **2014**, *26*, 4322. (m) He, Y. B.; Li, B.; O'Keeffe, M.; Chen, B. L. *Chem. Soc. Rev.* **2014**, *43*, 5618. (n) Zhou, H. C.; Kitagawa, S. *Chem. Soc. Rev.* **2014**, *43*, 5415. (o) Yan, Y.; Yang, S. H.; Blake, A. J.; Schroder, M. *Acc. Chem. Res.* **2014**, *47*, 296. (p) Eddaoudi, M.; Sava, D. F.; Eubank, J. F.; Adil, K.; Guillerm, V. *Chem. Soc. Rev.* **2015**, *44*, 228.

(7) (a) Vukotic, V. N.; Loeb, S. J. *Chem. - Eur. J.* **2010**, *16*, 13630. (b) Vukotic, V. N.; Loeb, S. J. *Chem. Soc. Rev.* **2012**, *41*, 5896. (c) Cao, D.; Juricek, M.; Brown, Z. J.; Sue, A. C. H.; Liu, Z. C.; Lei, J. Y.; Blackburn, A. K.; Grunder, S.; Sarjeant, A. A.; Coskun, A.; Wang, C.; Farha, O. K.; Hupp, J. T.; Stoddart, J. F. *Chem. - Eur. J.* **2013**, *19*, 8457. (d) Zhao, Y. L.; Liu, L. H.; Zhang, W. Y.; Sue, C. H.; Li, Q. W.; Miljanic, O. S.; Yaghi, O. M.; Stoddart, J. F. *Chem. - Eur. J.* **2009**, *15*, 13356. (e) Li, Q.; Sue, C.-H.; Basu, S.; Shveyd, A. K.; Zhang, W.; Barin, G.; Fang, L.; Sarjeant, A. A.; Stoddart, J. F.; Yaghi, O. M. *Angew. Chem., Int. Ed.* **2010**, *49*, 6751. (f) Li, Q.; Zhang, W.; Miljanic, O. S.; Knobler, C. B.; Stoddart, J. F.; Yaghi, O. M. *Chem. Commun.* **2010**, *46*, 380. (g) Zhu, K. L.; Vukotic, V. N.; O'Keefe, C. A.; Schurko, R. W.; Loeb, S. J. *J. Am. Chem. Soc.* **2014**, *136*, 7403. (h) Zhu, K. L.; O'Keefe, C. A.; Vukotic, V. N.; Schurko, R. W.; Loeb, S. J. *Nat. Chem.* **2015**, *7*, 514.

(8) Vukotic, V. N.; Harris, K. J.; Zhu, K.; Schurko, R. W.; Loeb, S. J. *Nat. Chem.* **2012**, *4*, 456.

(9) Loeb, S. J.; Tiburcio, J.; Vella, S. J. *Org. Lett.* **2005**, *7*, 4923.

(10) (a) Lin, X.; Telepeni, I.; Blake, A. J.; Dailly, A.; Brown, C. M.; Simmons, J. M.; Zoppi, M.; Walker, G. S.; Thomas, K. M.; Mays, T. J.; Hubberstey, P.; Champness, N. R.; Schroeder, M. *J. Am. Chem. Soc.* **2009**, *131*, 2159. (b) Perman, J. A.; Cairns, A. J.; Wojtas, L.; Eddaoudi, M.; Zaworotko, M. J. *CrystEngComm* **2011**, *13*, 3130. (c) Zhang, Z. J.; Wojtas, L.; Zaworotko, M. J. *Cryst. Growth Des.* **2011**, *11*, 1441. (d) Zhao, D.; Yuan, D. Q.; Yakovenko, A.; Zhou, H. C. *Chem. Commun.* **2010**, *46*, 4196.

(11) Nakazono, K.; Takata, T. *Chem. - Eur. J.* **2010**, *16*, 13783.

(12) (a) Larsen, R. W.; McManus, G. J.; Perry, J. J.; Rivera-Otero, E.; Zaworotko, M. J. *Inorg. Chem.* **2007**, *46*, 5904. (b) Perry, J. J.; Kravtsov, V. C.; McManus, G. J.; Zaworotko, M. J. *J. Am. Chem. Soc.* **2007**, *129*, 10076. (c) Wang, H. N.; Meng, X.; Yang, G. S.; Wang, X. L.; Shao, K. Z.; Su, Z. M.; Wang, C. G. *Chem. Commun.* **2011**, *47*, 7128. (d) Li, M.; Li, D.; O'Keeffe, M.; Yaghi, O. M. *Chem. Rev.* **2014**, *114*, 1343.

(13) Li, C. Q.; Qiu, W. G.; Shi, W.; Song, H. B.; Bai, G. M.; He, H.; Li, J.; Zaworotko, M. J. *CrystEngComm* **2012**, *14*, 1929.

(14) (a) Abourahma, H.; Coleman, A. W.; Moulton, B.; Rather, B.; Shahgaldian, P.; Zaworotko, M. J. *Chem. Commun.* **2001**, 2380. (b) Moulton, B.; Lu, J. J.; Mondal, A.; Zaworotko, M. J. *Chem. Commun.* **2001**, 863.

(15) (a) Wang, X. S.; Ma, S. Q.; Forster, P. M.; Yuan, D. Q.; Eckert, J.; Lopez, J. J.; Murphy, B. J.; Parise, J. B.; Zhou, H. C. *Angew. Chem., Int. Ed.* **2008**, *47*, 7263. (b) Liu, X. F.; Park, M.; Hong, S.; Oh, M.; Yoon, J. W.; Chang, J. S.; Lah, M. S. *Inorg. Chem.* **2009**, *48*, 11507.

(16) (a) Spek, A. L. *J. Appl. Crystallogr.* **2003**, *36*, 7. (b) Spek, A. L. *Acta Crystallogr., Sect. D: Biol. Crystallogr.* **2009**, *65*, 148.

(17) Sun, D. F.; Ma, S. Q.; Simmons, J. M.; Li, J. R.; Yuan, D. Q.; Zhou, H. C. *Chem. Commun.* **2010**, *46*, 1329.

(18) (a) Chandrakumar, N. *Spin-1 NMR*; Springer-Verlag: Berlin, 1996. (b) Schmidt-Rohr, S. H. W. *Multidimensional Solid-State NMR and Polymers*; Academic Press: New York, 1994.

(19) (a) Wittebort, R. J.; Olejniczak, E. T.; Griffin, R. G. *J. Chem. Phys.* **1987**, *86*, 5411. (b) Buchanan, G. W.; Moghimi, A.; Ratcliffe, C. I. *Can. J. Chem.* **1996**, *74*, 1437.

(20) Meirovitch, E. *J. Phys. Chem.* **1985**, *89*, 2385.

DOI: 10.1021/jacs.5b04674
J. Am. Chem. Soc. 2015, 137, 9643−9651